A Hardware-in-the-Loop Test Rig for Designing Near-Earth Aerial Robotics

Vefa Narli and Paul Y. Oh*

Drexel Autonomous Systems Lab, Philadelphia PA

vefa.narli@drexel.edu, paul.yu.oh@drexel.edu
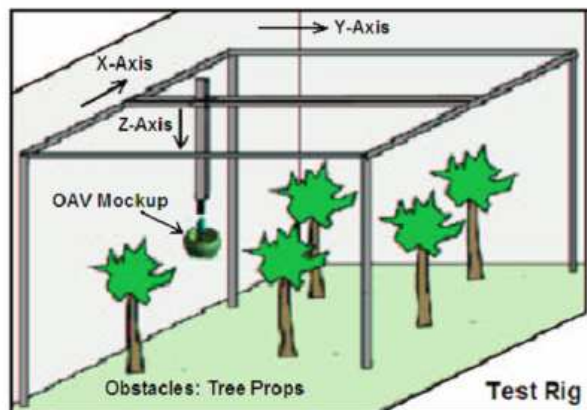
Abstract

Figure 1: Test rig concept drawing: The workspace is a full-scale diorama of a near-Earth environment like forests. The rig is used to capture metrics of aerial robot performance.

1   Introduction

Micro Air Vehicles are bird-sized autonomous flying aircraft designed to gather intelligence and provide situational awareness for soldiers and first responders. Called MAVs, such vehicles first began appearing in the late 1990s in fixed-wing configurations [3] [6]. Today's technical requirements are more demanding and entail flying autonomously in near-Earth environments like forests, caves, tunnels and buildings. To avoid confusion, such aircraft are often denoted as organic air vehicles (OAVs) or Class 1 or 2 Future Combat System (FCS) unmanned air systems. In the United States, DARPA and the Army have defined technical requirements such that the aerial robot performs hover- or perch-and-stare missions for reconnaissance, surveillance and target acquisition (RSTA). The net effect is that MAVs supporting platoon level missions today look and perform much differently from those fixed-wing variants that appeared five or more years ago.

Flying autonomously in near-Earth environments demands a sensor suite that can perform in cluttered areas where GPS often fails and communications are

degraded. Additionally, the sensor suite must operate day or night, despite adverse weather conditions and obscurants, like fog, rain or dust.

. Consequently, much of the integration of sensor and air vehicle has been ad hoc and happenstance. Metrics like resolution, dynamic range, bandwidth and signal-to-noise ratio are important parameters that are needed to compare one sensor to another.

To address this gap, a test rig that can repeatably and controllably capture performance metrics is being designed. The final rig will be a six degree-of-freedom gantry. Figure 1 is a concept drawing where the rig's workspace contains a full-scale diorama of the near-Earth environment.

Attached to the gantry is a non-flying mockup of the aerial robot that will be retrofitted with candidate collision avoidance sensors. The mockup emulates the motions of the real vehicle. Here, sensor data feeds

into a high-fidelity math model of the real-world aircraft. The math model is then realized by the gantry using model reference adaptive control. The test rig has rain machine, dust machine, fog system, fans and lamps to reproduce rain, gust and obscurants. The net effect is a hardware-in-the-loop system to capture metrics that expose aerial robot performance in places like forests and buildings. This is important because such metrics help fill the gap in the knowledge domain and provide an analytical framework to design near-Earth aerial robots and vertically advance the field.

Figure 2 is a photo sequence, captured by time-lapse video, of the test rig being constructed. The workspace's length, width and height spans $19 \times 18 \times 16$ cubic feets. Such dimensions can accomodate a full-scale diorama. Urban structures are near-Earth environments of pressing interest. As such, a two-story habitat commonly found in deserts was created. Figure 3 depicts the concept drawing and the realized diorama. Surrounding the top of the test rig there are 12 750 Watt rating lamps to emulate day and night conditions (Figure 3 right.) The rig also has a custom built rain machine as shown in the figure.

The test rig is a design in progress. The purpose of this paper is to introduce its current capabilities with some preliminary results as described in Sections 2 and 3 respectively. Section 4 concludes and discusses future work.

2 Test Rig Dynamics and Control

Table 1 is a typical flight envelope for flying in cluttered near-Earth environments as defined through various DARPA Industry Day briefings. The net effect is that the workspace is large enough to explore, test and evaluate sensor metrics in closed quarters; the vehicle will not be traveling quickly when performing missions like perch-and-stare.

Parameter	Value	Units
Horizontal Acceleration	9.6	ft/s^2
Horizontal Speed	2	ft/s
Vertical Acceleration	5	ft/s^2
Vertical Speed	10	ft/s

Table 1: Maximum speeds and accelerations for flying in near-Earth environments

2.1 Test Rig Dynamics

A XYZ gantry was custom built to meet the speeds and accelerations listed in Table 1. Its brushless DC motors position the gantry's arm. The maximum payload that the gantry can carry is 35 pounds. Table 2 lists the gantry's range-of-motion and fall closely the maximums listed in Table 1. Faster speeds and accelerations are possible but increase end-point vibrations because the gantry arm acts like a cantilever beam. Guy wires, clamping and adding weight are some avenues that can be explored to increase the specifications given in Table 2.

Parameter	Value	Units
X-axis range (length)	17.72	ft
X-axis speed	2	ft/s
X-axis acceleration	2.95	ft/s^2
Y-axis range (width)	13.84	ft
Y-axis speed	2	ft/s
Y-axis acceleration	3.69	ft/s^2
Z-axis range (height)	5.43	ft
Z-axis speed	2	ft/s
Z-axis acceleration	7.40	ft/s^2

Table 2: Gantry range-of-motion parameters. The values reflect using a 35 pound payload mounted on the gantry arm and suspended 2.72 feet off the ground.

2.2 Controller Structure

The controller structure of the test rig is shown in Figure 4. Two computers are used; one hosts the Data Acquistion Card (NI-6259 mDAQ) and the FPGA card (NI-7831R), while the other communicates with RTOS. The real time Labview code is run in the target computer at 25 kHz to control the gantry motors. The control input is sent to the amplifiers at 2.5 kHz after being filtered. The NI-7831R FPGA card is used to send PWM control signals to the amplifiers and to read encoder data. The NI-6259 mDAQ is used to capture real time sensor readings. The net effect is a deterministic hardware-in-the-loop system capable of storing real time test data. PID and state feedback controllers were succesfully implemented for positioning the gantry arm. In the Z-axis, integral control was a necessity to effectively implement gravity compensation.

Figure 2: Image stills from time-lapse recording of the rig's construction
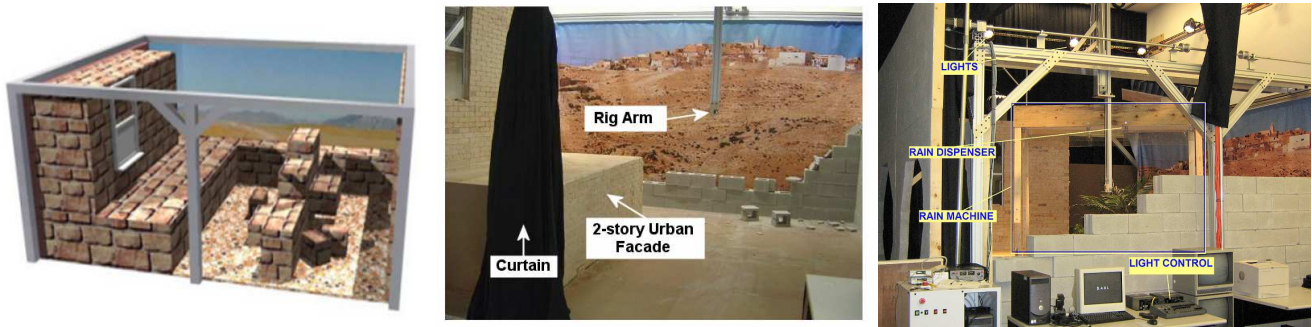

Figure 3: Urban Near-Earth Environments. Concept drawing (left), full-scale diorama (middle) and rain and light system of the test rig (right).
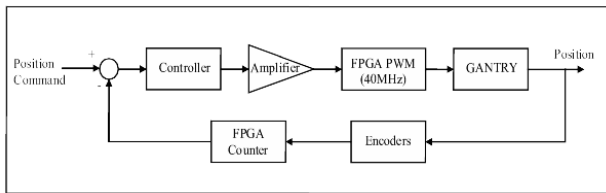

Figure 4: Test Rig's Controller Structure.

3   Trial Run - Sensor Calibration and Collision Avoidance

A number of studies are planned and include optic flow [1] [4] and acoustic sensors [5] as well as lidar, radar [2] and computer vision [7]. To establish the software infrastructure, and both data collection and calibration procedures, an off-the-shelf infrared (IR) sensor, Sharp GP2D02, was used. Its detection range is specified as 20 to 80 *cm*. This sensor generates an 8-bit value proportional to IR signal strength. A series of experiments were conducted to calibrate the IR sensor. The outcome is that a simple collision avoidance algorithm was run succesfully with the calibrated IR sensor in the loop.

3.1   IR Tests and Calibration

IR sensor ranging tests were conducted in the test rig workspace at constant temperature $(63.7 - 65.3°F)$ and lighting (45-50 Lux). Test objects included plywood, cinder blocks and steel rods painted in glossy white and black finishes. The objects to be detected were two 2×2 square foot piece of plywood, two cinder block with 0.5×1.5 square feet face and steel rods at different diameters as shown in Figure 5. The IR sensor was attached to the test rig's arm (Figure 5.) The gantry can accurately position the arm with respect to the object. As such, 800 range readings were taken at 3-inch intervals to capture IR sensor behavior.

According to its specifications, the Sharp GP2D02 outputs a nominal value (75 decimal) when no obstacle is in range. This was verified by performing 5 trials and plotted in Figure 6. Figure 6 reveals a Gaussian distribution as one would expect. The average of the readings is 75.6 and the standard deviation is 1.9. One would conclude that that there is an obstacle at some distance if the decimal reading is greater than 82. The probability that the sensor reading would be 82 (3σ) when there is no obstacle, is less than 0.15%. Therefore, 82 is the threshold value to flag a collision

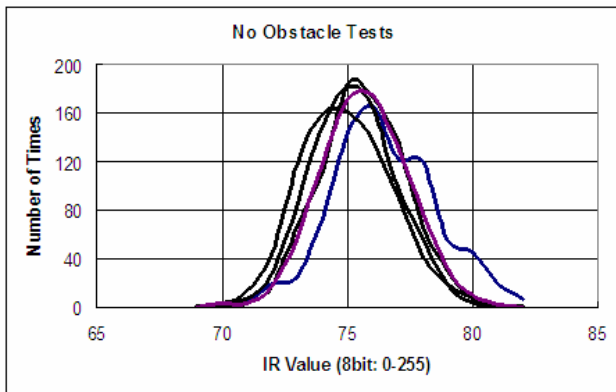Figure 5: IR Sensor Tests: plywood (left), cinder blocks (middle), steel rods (right)

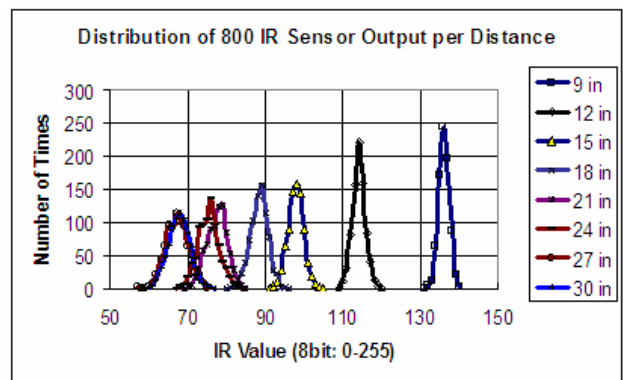Figure 6: IR sensor output with no obstacle in range.

Figure 7: Response to Glossy White Plywood: IR sensor output value versus distance to plywood.

avoidance algorithm.

Figure 7 depicts the response of the IR sensor when located at the shown distances from the plywood obstacle. Cinder block and steel rod tests were performed the same way and the averages of these tests are compared with the glossy white plywood response (Figure 8, Figure 9.)

The tests performed with plywood and cinder block objects revealed two things: one, black painting yields decreased IR sensor response; and two, IR sensor response to cinder block is somewhat lower than plywood (Figure 8.) One can conclude that IR sensor response depend on color and surface roughness of the obstacles.

Most sensors available to the aerial robotics community interact with their surroundings and with their environment even more dramatically than the response that was observed here. The test rig would be consequential in filling the gap in the sensor metric knowledge domain as well as meeting the need to
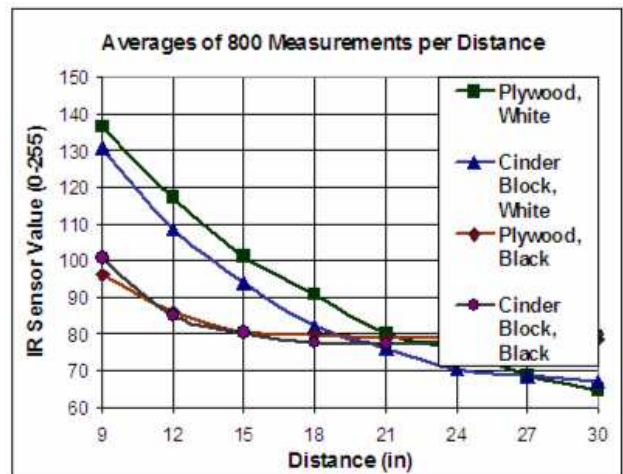

Figure 8: IR sensor output average value versus distance to object (plywood/cinder block).
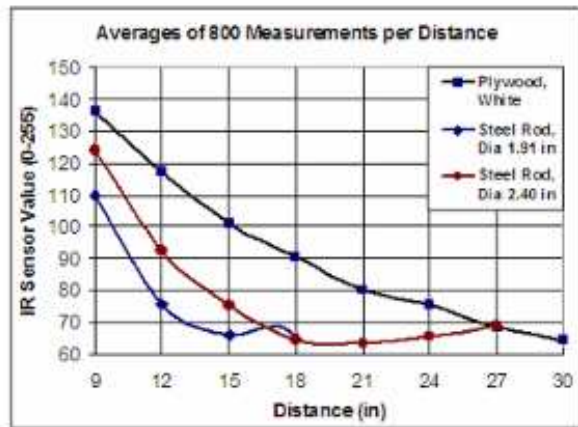
Figure 9: Response to Steel Rod: IR sensor output value versus distance to white steel rod, compared to plywood tests.

expose aerial robot performance in near-Earth environments.

3.2 Collision Avoidance

Applying factorial design, where one parameter is adjusted while others are frozen, results in a large amount of data. For Gaussian distributions, the three sigma point can be used to be highly confident if an obstacle is present. In the previous section, IR range data for plywood, cinder blocks and steel rods were given. As such, a 2.4 inch wide object, ranging 12 inches away or less, can be reliably detected. Figure 9 shows that as small as a 2.4 inch diameter rod at $9 - 12$ inches distance can be detected with the IR sensor, remembering that the threshold for a reliable reading is 82 (decimal IR output).

To demonstrate a hardware in the loop test, a collision avoidance algorithm was designed and tested using the IR sensor. The math model of the aerial robot will be flaged by a similar collision avoidance algorithm using real sensors like lidar, vision and optic flow attached on the full scale mockup of the robot.

Figure 10 shows how the collision avoidance algorithm moves the gantry around the plywood obstacle. It sends a new target position command to the controller until it is safe to redirect the gantry to the original target position. Initial position was chosen as (0, 0, 0) and the gantry was commanded to (70 in, 0 in, 0 in). The plywood obstacle was positioned on the diorama such that its center is at (48in, 6in, 6in). The
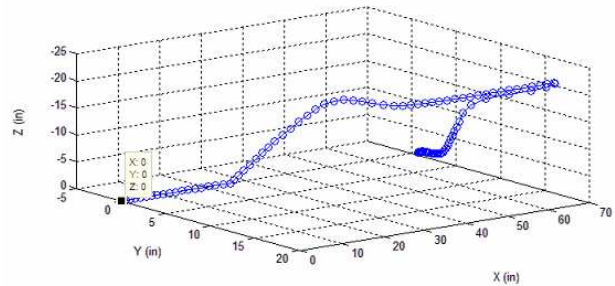

Figure 11: Collision Avoidance Test

three-dimensional path of the gantry arm is shown in Figure 11.

4 Conclusions and Future Work

In the United States, congress has mandated that one third of all fighter aircraft are to be unmanned by the year 2015. With less than a decade remaining, there are unresolved gaps that must be addressed. One gap that prevents a vertical advance in the field of near-Earth aerial robotics is the lack of sensor suite performance metrics. Absent in the knowledge domain are metrics like resolution, range, signal-to-noise ratios and dynamic response for sensors performing in areas like forests, caves, tunnels and buildings. Without such metrics, integration of sensor suite and aircraft is happenstance and performance is circumspect.

The aerial robotics test rig with its diorama, rain and dust machine, lighting generator, and real time data feedback capability will be consequential in meeting the need to expose aerial robot performance in near-Earth environments.

Preliminary illustration of the rig's capabilities was demonstrated by using an IR sensor. Here, factorial design was used to ascertain data points that yield a high probability of detecting obstacles. Additional sensors like optic flow, lidar and sonar are actively being pursued. Future work is to model such sensors; two, incorporate vehicle dynamics into a model reference adaptive controller; three, implement and evaluate the performance of collision avoidance strategies like weighted node and reactive path planning.

References

[1] Barrows, G., Neely, C. . "Mixed-mode VLSI Optic Flow Sensors for In-flight Control of a Micro Air Vehicle", , 4109 pp. 52-63, 2000.
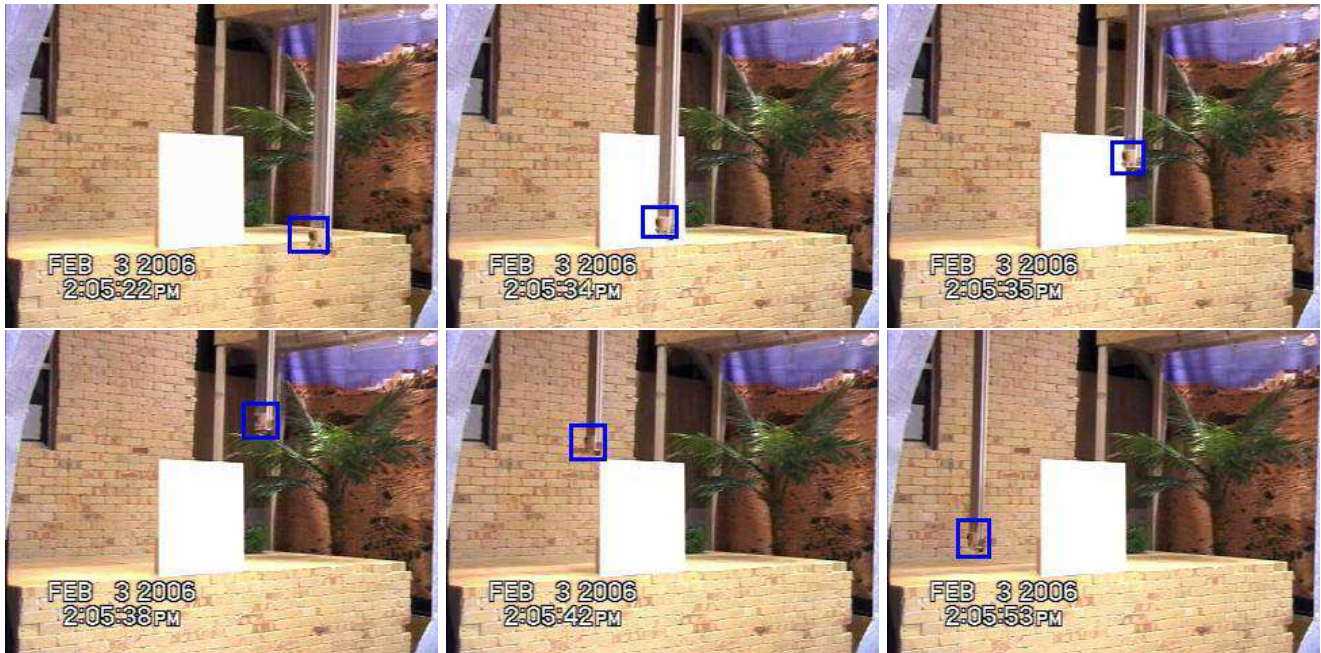
Figure 10: The IR sensor on the mockup must detect the vent on the facade's roof. Sequential photos (left to right, top to bottom) of mockup relative to the vent.

[2] Fontana, R.J., et al, "An Ultra Wideband Radar for Micro Air Vehicle Applications",

, pp. 187-191, 2002.

[3] Grasmeyer, J.M., Keennon, M.T. . "Development of the Black Widow Micro Air Vehicle",

, Reno, NV, 2001.

[4] Green, W.E., Oh, P.Y., Barrows, G. . "Flying Insect Inspired Vision for Autonomous Aerial Robot Maneuvers in Near-Earth Environments,"

(ICRA), New Orleans, V1, pp. 2347-2352, 2004.

[5] Horiuchi, T., Hynna, K., "A VLSI-based Model of Azimuthal Echolocation in the Big Brown Bat", , V11 N3, pp. 241-247, 2001.

[6] Kellogg, J., et al. "The NRL MITE Air Vehicle",

, Bristol, UK, 2001.

[7] Pipitone, F., Kamgar-Parsi, B., Hartley, R. . "Three Dimensional Computer Vision for Micro Air Vehicles",

, Conf. 4363, Enhanced and Synthetic Vision 2001, Orlando Florida, 2001.